Density-functional theory applied to Rh(111) and CO/Rh(111) systems: Geometries, energies, and chemical shifts

M. Birgersson* and C.-O. Almbladh†
Department of Solid State Theory, Institute of Physics, Lund University, Sweden

M. Borg‡ and J. N. Andersen§
Department of Synchrotron Radiation Research, Institute of Physics, Lund University, Sweden

(Received 10 July 2002; revised manuscript received 15 October 2002; published 14 January 2003)

We present extensive density-functional theory (DFT) based calculations of the clean Rh(111) surface and of CO/Rh(111) overlayer systems. We study both ground-state structural properties and core-level shifts from differences in total energies at different coverages and adsorption sites. Most results are obtained using using norm-conserving or ultrasoft pseudopotentials. The overall reliability of the pseudopotential method is analyzed theoretically, and computationally by way of all-electron calculations. In general, core corrections are required in order to correctly simulate all-electron total energies, although the corrections are rather small for the systems considered here. Overall there is a very good agreement both between the pseudopotential and all-electron results as well as with high-resolution experimental spectra. The obtained agreement between theoretical and experimental core-level energies, however, requires that the correct geometrical parameters are used. For instance, inclusion of bucklings of the first Rh layer in the (2×2)-1CO and $(\sqrt{3}\times\sqrt{3})R30°$-1CO overlayers is essential. For the overlayers studied here, different competing adsorption sites give almost the same frozen-lattice adsorption energies. However, the C 1*s* binding energy shows large differences between CO adsorbed in different sites. Thus calculations of the C 1*s* shifts allow us to predict the adsorption sites despite the small differences in ground-state energies. We also analyze sources of the shifts in terms of differences in Hartree potential and relaxation at different sites. As the DFT core eigenvalue lies above rather than below the core excitation energy some care is required in order to properly identify a relaxation energy in a DFT framework. In order to clarify the question we relate the DFT approach for core energies to approaches based on self-energies or the Hartree-Fock approximation.

DOI: 10.1103/PhysRevB.67.045402 PACS number(s): 68.43.Bc, 68.43.Fg, 71.15.Mb, 79.60.Dp

I. INTRODUCTION

Density-functional theory[1,2] (DFT) has developed into an extremely useful tool for making realistic simulations of complex systems like solid surfaces and adsorbates at surfaces. In its original form it is applicable only to ground-state properties such as geometries and total energies. However, it is known since many years ago that also energies of fully relaxed core-hole states can be rather successfully modeled by DFT (for overviews, see, e.g., Refs. 3 and 4). The capabilities of *ab initio* simulations combined with experimental techniques such as high-resolution core-level spectroscopy (HRCLS) make it possible to determine local geometric and electronic structure, vibrational properties, and other properties with high accuracy. A major aim of the present paper is to combine state-of-the art HRCLS results on Rh(111) and CO adsorbed on Rh(111) with detailed DFT simulations in order to obtain conclusive evidence on how the CO molecule adsorbs at different coverages. We believe that it is extremely useful to combine computational and experimental techniques. For instance, we find that core-level shifts often depend on the geometrical structure such as layer relaxation in a rather sensitive way. Thus by combining experimentally determined shifts with theoretical calculations one may obtain very precise information. Another aim of the present work is to shed light on the overall reliability of DFT-based calculations of core-level spectra and the major approximations involved.

The Rh(111) and CO/Rh(111) systems have experimentally been extensively and increasingly studied during the last 30 years with a large number of different techniques. The Rh/CO system has been chosen both because of its industrial applications in forms of catalysis and because CO adsorption has become a test case for molecular absorption on metal surfaces in general. Examples of investigation techniques are thermal desorption spectroscopy (TDS),[5] low-energy electron diffraction (LEED),[6] electron energy-loss spectroscopy (EELS),[7] surface x-ray diffraction (SXRD),[8] helium atom scattering (HAS),[9] and high resolution core level spectroscopy (HRCLS).[10] A wealth of experimental results are thus available for this system.

Over the years there have been several calculations with different degree of sophistication performed to support experiments concerning core level shifts on Rh surfaces. In the early 1980s Feibelman[11] made a calculation using a linear combination of atomic orbitals (LCAO) approach of the surface core-level shift (SCLS) for a clean Rh(111) surface and a Rh(111) surface with a carbon overlayer. In the 1990s, *ab initio* calculations applied to surfaces and adsorbates appeared. Methfessel *et al.*[12] investigated the surface relaxation for Rh(111) among other 4*d* metal surfaces using a DFT-based full potential linear muffin-tin orbital (LMTO) method.[13] Using the same computational tools the SCLS for Rh(111) and other 4*d* metal surfaces were later investigated by Andersen *et al.*[14] Further structural investigations of the clean Rh(111) system were performed by Eichler *et al.*[15] and

more recently the adsorption of CO on Rh(100) was thoroughly investigated by Eichler and Hafner.[16]

In this paper we present an extensive set of calculations made to support experiments performed on the clean Rh(111) and CO/Rh(111) systems at MAX-lab by some of us.[17,10,18] In these experiments CO covered rhodium surfaces are studied with HRCLS and LEED. Several ordered overlayer structures have been found and their behavior with varying temperature and pressure has been determined. Specifically, below 120 K, stable structures of absorbed CO have been found at coverages of 0.25 [a (2×2) structure with adsorption on top], 0.33 [a $(\sqrt{3}\times\sqrt{3})$ structure with adsorption on top], and 0.75 [a (2×2)-3CO structure with adsorption both in on-top and hollow positions] monolayers (ML's). Different structures have also been found at intermediate coverages (0.5–0.75 ML's) but in this paper we will focus on the first three mentioned.

The structure of the paper is as follows. We start by giving a theoretical background including an analysis of the relation between DFT and self-energy methods and a discussion of additional corrections which may arise from using pseudopotentials (Sec. II). Next, in Sec. III, we present the actual systems which have been calculated, followed by a discussion of the results. This section is divided into two parts, discussing separately geometrical features and chemical shifts in these systems. In Sec. IV we give our conclusions.

II. THEORY

A. Core-electron photoemission

In core-level photoemission a core electron is removed from the system by a photon (usually in the x-ray regime) and leaves the solid to get its kinetic energy and possibly its momentum measured in a detector. The difference between the energy of the in-going photon and the kinetic energy of the electron gives directly the excitation energy of the system left behind. In the most simple-minded one-electron picture the core-electron spectrum would consist of a sharp line at the core-electron energy ϵ_c. In reality, the system can be excited to many different final states, and the core spectrum therefore consists of a peak of a certain width, the core-electron quasiparticle, and usually also satellites at higher binding energies. Owing to the negligible bandwidth and usually rather long hole lifetime, the core-electron spectrum has a special structure with a more or less well-defined high-energy threshold corresponding to a fully relaxed core-hole state $|0^*\rangle$. We take the position of this high-energy threshold as the definition of the core-electron energy,

$$\epsilon_c = E_0(N) - E_0{}^*(N-1). \tag{1}$$

Although in reality an excited state, the fully relaxed core-hole state is rather similar to a ground state as far as the valence electrons are concerned. It it well established through many works (see, e.g., Refs. 14 and 19–21) that the valence-electron relaxation is well described by ground-state DFT. Some formal justification for using DFT to obtain core shifts may be obtained by considering constrained minimization in subspaces corresponding to different configurations of a particular ion core in the solid. Such a procedure would lead to density functionals which depend parametrically on the ion core configuration. This dependence, however, is highly transferable and may be estimated using some reference system such as an isolated atom. When comparing core-electron energies of the same kind of atoms in different environments, as is the case when calculating core-level binding energy shifts, the core configuration dependence in the density functional cancels to high accuracy. The similarity between ground states and fully relaxed core-hole states also underlies the successes of the equivalent-core approximation[22,23] where an ionized ion core Z is approximated by a ground-state core, $Z+1$.

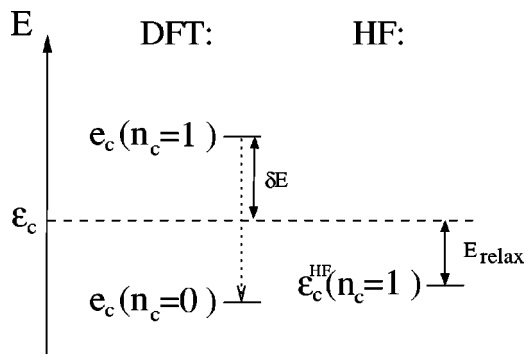

FIG. 1. Relation between HF and DFT eigenvalues and excitation energies for deep core states. The dotted arrow indicates the movement of the DFT eigenvalue as the core state is emptied. The energy difference δE has no physical relevance.

B. Core-hole relaxation from DFT and from self-energies

Core-level shifts in solids and at solid surfaces are often discussed in terms of ''initial-state'' and ''final-state'' parts where the initial-state part is connected with the shift in core-electron orbital eigenvalue, and where the final-state (relaxation) part contains the remaining contributions. The terminology originates from Hartree-Fock (HF) ''ΔSCF'' methods in which the core-electron energy is approximated by two separate calculations as in Eq. (1). However, the HF and DFT orbital eigenvalues have rather different relations to total-energy differences,[24] as depicted in Fig. 1. The Hartree-Fock eigenvalue lies *below* the ΔSCF results and, for deep core levels, also below the true excitation energy. The difference between the excitation energy $\epsilon_c = [E_0(N) - E_0^*(N-1)]$ (as obtained by the HF approximation) and the HF eigenvalue ϵ_c^{HF} is usually termed relaxation energy. This energy, which is always positive, has the physical interpretation of being the energy gained by the system as a result of the core-hole induced relaxation of the orbitals. Contrary to HF, the DFT eigenvalue lies initially *above* the excitation energy and the local-density approximation (LDA) to the eigenvalue even higher. Both move downwards when the core level is emptied and are below the excitation energy in the final-state configuration.[58] The difference(s) between the DFT eigenvalue(s) and the true excitation energy has no direct physical interpretation. As will be shown in the follow-

ing, it is, however, possible to define a relaxation energy in DFT which has a similar physical interpretation as in the HF approximation.

Within Hartree-Fock theory, the problem of core-level shifts and shake up has been discussed in classical papers by Hedin and Johansson,[25] and by Manne and Åberg.[26] According to Hedin and Johansson, the core-electron energy as obtained from the difference between two separate Hartree-Fock total-energy calculations can be written

$$\epsilon_c = \epsilon_c^{HF} + \frac{1}{2}\langle c|V_p|c\rangle \tag{2}$$

in terms of the HF eigenvalue ϵ_c^{HF} with filled core level, and the core-hole induced change V_p in Hartree and exchange potential. (V_p is usually termed 'polarization potential.'') The above result is closely related to the results from the dynamically screened exchange or ''GW'' approximation to the self-energy Σ,[27]

$$\epsilon_c = \epsilon_c^0 + \langle c|V_C'|c\rangle + \langle c|\Sigma_v^x|c\rangle + \frac{1}{2}\langle c|V_p^v|c\rangle. \tag{3}$$

In Eq. (3), ϵ_c^0 is the core-electron energy of the free ion, V_C' the Coulomb potential from valence electrons and surrounding nuclei, Σ_v^x is the valence contribution to the exchange potential, and V_p^v the polarization potential from only valence electrons. The first three terms account for the HF eigenvalue plus the intracore part of the polarization potential in Eq. (2). The remaining valence-electron part of the polarization potential is accounted for by V_p^v.

In order to make contact with DFT, we identify ϵ_c with the total-energy difference $E(n_c=0)-E(n_c=1)$ and make use of the identity[19,28]

$$e_c(n_c) = \partial E_c(n_c)/\partial n_c$$

(e_c and n_c are the core-electron DFT eigenvalue and occupation number, respectively). We express the core-electron energy for the free ion in an analogous way and obtain

$$\epsilon_c = \epsilon_c^0 + \int_0^1 \{e_c(n_c) - e_c^0(n_c)\} dn_c\,. \tag{4}$$

(We use superscript ''0'' for free-ion quantities.) To good accuracy we may neglect the difference in shape of core orbitals in the ion and in the solid. Making use of this approximation, we can rewrite the eigenvalue difference in Eq. (4) as

$$e_c - e_c^0 = \langle c|V_C - V_C^0 + v_{xc} - v_{xc}^0|c\rangle. \tag{5}$$

Now, $V_C - V_C^0$ equals the Coulomb potential from valence electrons and surrounding nuclei V_C'. As before we introduce a polarization potential $V_p^v(n_c) = V_C'(n_c) - V_C'(1)$. We make a corresponding separation of the exchange-correlation part $\Delta v_{xc}(n_c) = v_{xc}(n_c) - v_{xc}^0(n_c)$ into an initial-state part $\Delta v_{xc} \equiv \Delta v_{xc}(1)$ and a core-hole induced part $\Gamma(n_c) = \Delta v_{xc}(n_c) - \Delta v_{xc}(1)$ to obtain

$$\epsilon_c = \epsilon_c^0 + \langle c|V_C'|c\rangle + \langle c|\Delta v_{xc}|c\rangle + \int_0^1 \{\langle c|V_p^v(n_c) + \Gamma(n_c)|c\rangle\} dn_c\,. \tag{6}$$

By splitting off the core-electron energy of a reference system, direct reference to the unphysical DFT eigenvalue has been eliminated. Comparing with the GW result in Eq. (3) we see that the first two terms are unchanged, while in the DFT approach the core-valence exchange is accounted for by Δv_{xc}. The first three terms are properly regarded as the solid-state contribution to the 'initial-state' part. In the core-hole induced last term we see that the polarization contributions agree to linear-screening order but that DFT accounts also for nonlinear screening effects that would require vertex diagrams beyond GW. In addition, Eq. (6) also accounts for core-hole induced changes in core-valence exchange, which again simulate vertex contributions beyond GW theory.

In summary, while the quantity

$$[E^{\text{solid}}(1) - E^{\text{solid}}(0)] - e_c^{\text{solid}} = \epsilon_c^{\text{solid}} - e_c^{\text{solid}}$$

has no physical meaning and could not be associated with a relaxation energy in a DFT scheme, the quantity

$$\Delta E_{\text{relax}} = \epsilon_c^{\text{solid}} - e_c^{\text{solid}} - [\epsilon_c^{\text{ref.}} - e_c^{\text{ref.}}],$$

where a reference system has been singled out, behaves as expected and could be used as the definition of the relaxation energy shift when going from the reference system to the solid. If we consider core *shifts* rather than absolute core energies, the reference system will not enter meaning that *shifts* in DFT eigenvalues reflect initial-state shifts.

C. Core corrections in the pseudopotential approach

In this work we mainly use plane waves and norm-conserving or ultrasoft pseudopotentials[29,30] for computing core-level shifts. Such potentials ensure good transferability of eigenvalues and of charges and potentials outside the core region. The total energy, however, involves directly the pseudopotential and the pseudocharge also in the core regions, where they have no direct physical meaning. As a consequence, one must in general add core corrections in order to obtain correct and transferable total energies in pseudopotential schemes.[31,32]

In a norm-conserving pseudopotential scheme, the DFT eigenvalue $e_c(n_c)$ corresponds to the derivative of the total energy with respect to n_c. The total energy is variational, and thus we only need to take the explicit n_c dependence into account when evaluating the derivative. Thus

$$\frac{\partial E_{ps}(n_c)}{\partial n_c} = \int \rho_{ps} \frac{\partial w_{ps}^0}{\partial n_c} - \sum_{j\neq 0} Z_v^j \frac{\partial w_{ps}^0}{\partial n_c}, \tag{7}$$

where the last term arises from the Coulomb interaction between the pseudopotentials themselves. [In Eq. (7), w_{ps}^i is the pseudopotential for atom ''i,'' Z_v^i the charge of the corresponding ion core, and ρ_{ps} is the density of pseudo charge. We temporarily suppress the l dependence of w_{ps}^0 in the core region.] In the second term we can replace $\partial w_{ps}^0/\partial n_c$ by $1/r$,

and thus we see that this term represents the Coulomb potential $V_C^{ion}(0)$ at the origin from surrounding ion cores. The integral in the first term in Eq. (7) we split into a contribution from the cell Ω_0 and a remainder. Owing to the norm-conserving properties of w_{ps}, this remainder when combined with the last term gives an accurate representation of the total Coulomb potential from all but the central cell. This part ΔV of the potential has no sources in the core region. Thus $\Delta V(0)=\langle c|\Delta V|c\rangle$, and

$$\frac{\partial E_{ps}(n_c)}{\partial n_c}=\langle c|V_C'|c\rangle+\int_{\Omega_0}\rho_{ps}\frac{\partial w_{ps}^0}{\partial n_c}-\int_{\Omega_0}\int_{\Omega_0}\frac{\rho_v(\mathbf{r})|\phi_c(\mathbf{r}')|^2}{|\mathbf{r}-\mathbf{r}'|}=\langle c|V_C'|c\rangle+\sum_l\int\left\{\rho_{ps}^{(l)}\frac{\partial w_{ps}^{(l,0)}}{\partial n_c}-\rho_v^{(l)}V_H^c\right\}, \tag{8}$$

where V_H^c is the Hartree potential from the core orbital in question, ρ_v is the true valence electron density, and where we have restored the l dependence of w_{ps}. In last term above, both V_H^c and $\partial w_{ps}/\partial n_c$ equal $1/r$ outside the core region. The integration is thus confined to $r<r_c$. Comparing with Eq. (5) we see that

$$e_c-e_c^0-\frac{\partial E_{ps}(n_c)}{\partial n_c}=\langle c|v_{xc}-v_{xc}^0|c\rangle+\sum_l\int\left\{\rho_v^{(l)}V_H^c-\rho_{ps}^{(l)}\frac{\partial w_{ps}^{(l,0)}}{\partial n_c}\right\}. \tag{9}$$

The terms on the right-hand side of Eq. (9) are sensitive to first-order changes of the density in the core region and are not transferable.

Of course one would like to estimate the correction above without actually doing all-electron calculations. To a first approximation one may then neglect the change in shape of the all-electron orbitals when going from the reference state to the solid. The density in the core region may then be obtained from the computed symmetry-decomposed pseudocharge density and the atomic orbitals in the reference state.

In order to estimate core corrections for the systems studied here we have performed all-electron calculations and evaluated the correction according to Eq. (9) for some important cases, namely the Rh 3d surface shift and the C 1s shifts at high coverage [(2×2)-3CO system]. In the case of Rh we find a surface shift of -0.46 eV from (full-potential) linearized augmented plane wave (LAPW) (Ref. 13) calculations, -0.50 eV from norm-conserving pseudopotentials, and a correction from Eq. (9) of about 0.03 eV. In the case of C 1s we use a rather small pseudopotential radius r_c, and as a result the core corrections are also smaller and below our computational accuracy. The smallness is partly due to a cancellation between the Hartree and exchange-correlation contributions in the correction formula above.

D. Computational details

In our plane-wave calculation we used both norm-conserving (NC) and ultrasoft pseudopotentials[33–35] and codes developed by Bockstedte *et al.*[29] and by Hammer *et al.*[30] The pseudopotentials were constructed using the free atoms in their ground configurations or in their core-excited neutral configurations as reference states. The core-level shifts were calculated as total-energy differences with and without a core hole as in Eq. (1).

In most of our calculations we used a generalized gradient approximation (GGA) to exchange and correlation. For the GGA we used the PW91 version.[36] In some tests the LDA was used. As will be seen in the next section, the calculated chemical shifts are rather sensitive to the detailed atomic geometry. The general experience is that GGA's usually improve structural properties like bond distances and geometries compared to LDA. For the systems we consider, GGA in the PW91 form indeed gives core shifts in better agreement with experiment than the LDA. This is, however, mainly a result of GGA providing a better determination of the geometrical parameters. For a given lattice geometry, we find that the LDA and the PW91 form of GGA give very similar core-level shifts.

In order to check the overall reliability of the pseudopotential approximation, we also performed LAPW-based all-electron calculations using LDA for some representative cases. The all-electron and plane-wave (norm-conserving) results for C 1s and Rh 3d agree within $\sim$50 meV or better. The difference between the all-electron and pseudopotential results is thus small, and it is well accounted for by the simplified formula in Eq. (9). The all-electron calculations also allow us to decompose the core-level shifts in initial and final-state parts by way of Eq. (7). An all-electron method is preferable in particular for d-electron systems. However, our tests show that the less expensive plane-wave calculations are of sufficient accuracy and not distorted by systematic errors related to the pseudopotential approximation.

In the calculations we model the surface by repeated slabs separated by vacuum layers. Important numerical parameters include (i) choice of pseudopotentials, (ii) basis set size, (iii) slab thickness, (iv) size of surface unit cell, (v) vacuum layer depth, and (vi) choice of integration method in k space.

In order to determine the core radius r_{cl} of the norm-conserving potentials some transferability tests were performed. The r_{cl} value for Rh was determined by comparing changes in total energies upon a doubling of the lattice constant. The radii were lowered until these changes had a negligible r_{cl} dependence. The parameters for C and O atoms were determined in a similar fashion by considering RhC and CO molecules and energy changes when the bond length was doubled. The transferability was considered converged when changes less than 0.02 eV were found upon further lowering of the r_{cl} values. The r_{cl} values determined for ground-state atoms were also used for modeling the core-excited atoms.

In the case of ultrasoft potentials we used predetermined potentials as distributed with the Dacapo code for the ground-state atoms. We constructed the potentials for core-excited atoms using the same parameters as for the corre-

sponding ground-state atom. We verified that the ultrasoft and norm-conserving potentials gave the same dependence of total energy on atomic distances in our transferability tests described above. We also compared with corresponding all-electron results.

The $4d$ electrons in Rh give a rather hard NC pseudopotential. The C and O atoms lack core electrons of p symmetry, and as a consequence the NC potentials for these atoms are even harder. Consequently, the NC potentials required very large basis sets. It turned out that the O potential was the hardest and necessitated a high cutoff of 85 Ry ($\sim$1160 eV). As expected, the ultrasoft potentials required a much lower cutoff of approximately 25 Ry (340 eV).

In order to test the overall reliability of the repeated slab approximation we performed calculations on both inversion-symmetric slabs with a CO molecule on each surface and dipole-corrected asymmetric slabs with the molecule on only one of the slab surfaces. For details of the dipole correction we refer to Refs. 29 and 37. We performed tests with up to seven layers in the symmetric case and five layers in the dipole-corrected case. Although we were not able to go beyond seven layers our results indicate a convergence within 30–50 meV for total energies and $\sim$20 meV for total energy differences (core energies, etc.). For more sensitive quantities, as for instance adsorption and surface energies, there are indications that quantum size effects affect the results up to approximately a slab thickness of 10-Rh layers.[15] Our tests indicate that the core-level shifts converge more rapidly with respect to slab size. In a similar way we verified that a (2×2) surface cell is a good approximation for modeling a isolated adsorbed CO molecule. The symmetric slabs were needed not only for convergence tests but also for determining the surface core shifts. In these calculations, the bulk was approximated by the middle layer and the slab becomes symmetric. In order to have as much cancellation of errors as possible with regard to, e.g., k-point integration it is important to use the same geometry and parameters for core holes in the bulk and the surface.

When it comes to the depth of the vacuum layer, its size will be determined by long-range multipole contributions to the surface potential. For a completely flat jellium surface, the potential tends to its vacuum value exponentially, but any corrugation will contribute multipoles with much slower fall-off. Consequently, a surface with an adsorbed molecule requires a thicker vacuum layer than does the clean surface. By varying the thickness we found that for the CO covered surfaces a thickness corresponding to 5-Rh layers was converged to within 0.03 eV for total energies.

The k-point integration was performed in the usual way using Monkhorst-Pack[38] points and Fermi-surface smearing and back extrapolation.[39] For the (2×2) surface unit cell a k-point mesh of $(4\times4\times1)$ was found to be accurate to about 0.02 eV.

For the supporting LAPW calculations, finally, we used local s orbitals on C and O and local d orbitals on the Rh atoms in order to improve convergence with respect to basis set size and to minimize linerarization errors. Again we used a Monkhorst-Pack k mesh and the tetrahedron method with a leading-order Fermi-surface correction by Blöchel *et al.*[40]

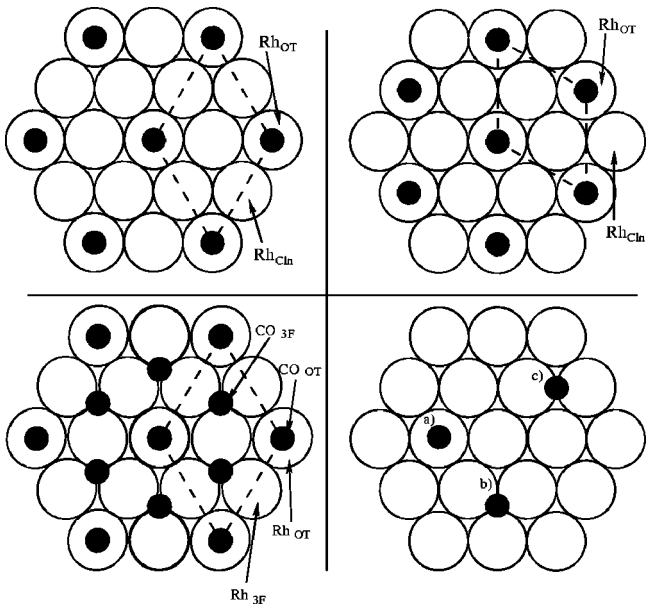

FIG. 2. The (2×2)-1CO (upper left panel), the $(\sqrt{3}\times\sqrt{3})R30°$-1CO (upper right), and the (2×2)-3CO (lower left) systems. The surface unit cells are indicated. The lower left panel shows the adsorption sites considered in our calculations: (a) on-top; (b) threefold hollow; (c) bridge.

III. RESULTS AND DISCUSSION

We focus on four different systems; the clean Rh(111) surface, the (2×2)-1CO system (which corresponds to a coverage of 0.25 ML), the $(\sqrt{3}x\sqrt{3})R30°$-1CO system (0.33 ML) and finally the (2×2)-3CO system (0.75 ML). The three latter systems can be seen in Fig. 2. In the following discussion we will distinguish between the high coverage limit, which corresponds to the (2×2)-3CO system while the low coverage limit refers to the 0.25- and 0.33-ML systems. We will start by discussing the geometrical features of these systems, then continue with the energy shifts of the Rh $3d$ and C $1s$ levels. The results are summarized in Tables I–X.

A. Geometries

Before treating the different rhodium surfaces, some bulk properties were calculated. Due to the use of GGA we, as expected, find a small overestimate of the bond lengths. The bulk lattice constant was calculated to 3.83 Å, slightly larger than the experimental value of 3.80 Å.[44] By fitting computed total energies at different lattice parameters, the bulk modulus was determined to 2.87 Mbar which agrees reasonably well with the experimental value 2.71 Mbar.[44] These bulk properties also agree well with those calculated in Refs. 15 and 16. The calculated bulk lattice parameter was used for the inner layers in the slab describing the Rh(111) surface.

1. Clean surface

The geometry for the clean Rh(111) surface was optimized by relaxing the two top-most layers. The full results of this calculation can be found in Table I. The result was a

TABLE I. Optimum geometrical parameters of the clean Rh(111) surface. The distances are depicted in Fig. 3. The relaxation Δd_{ii+1} is defined as $\Delta d_{ii+1} \equiv (d_{ii+1} - d_{\mathrm{Bulk}})/d_{\mathrm{Bulk}}$ where d_{Bulk} is the interlayer distance in the bulk crystal.

	Calculated value	Experimental value	Code
GGA lattice constant	3.83 Å	3.79 Å [a]	fhi98md
		3.80 Å [b]	
Δd_{12}	−1.5%	$-1.28\% \pm 0.9\%$ [a]	fhi98md
		$-1.37\% \pm 0.9\%$ [c]	
		$-3.0\% \pm 1.4\%$ [b]	
Δd_{23}	−1.0%	$-1.28 \pm 1.8\%$ [a]	fhi98md

[a]Reference 41.
[b]Reference 42.
[c]Reference 43.

small inward relaxation of both planes by 1.5 and 1.0%, respectively. These figures agree with other GGA calculations,[15] and also reasonably well with LMTO calculations made on the LDA level.[14,12] As can be seen in Table I our calculations also agree well with experimental values. It should be noted, however, that these experimental results have large uncertainties.

2. Low coverage limit

A most fundamental property of a molecular adsorption system is the adsorption site. Therefore we first calculate relative adsorption energies of the two low coverage overlayers for CO adsorbed in the three high-symmetry sites in order to test if DFT can reproduce the experimental result of adsorption only in on-top sites at low coverages.[6,7,10] The high symmetry sites can be seen in Fig. 2. This calculation will also serve as a crucial test for the approximation of DFT used, as pointed out by Feibelman *et al.*[45] (see Fig. 3). These authors showed that GGA predicts adsorption sites of CO on Pt(111) which are wrong in comparison with experiment irrespective of the computational technique used (pseudopotential vs all-electron, plane waves vs localized basis set, etc.). They argued that the LDA and the current GGA's tend to favor adsorption in sites of high molecule-substrate coordination.

As shown in Table II, in a (2×2)-1CO overlayer the threefold hollow site (hcp) is energetically favored by 46 meV over an on-top site whereas a bridge site is disfavored compared to the on-top site by 73 meV. For the $(\sqrt{3}\times\sqrt{3})R30°$ overlayer, the ordering of the on-top and hollow adsorption sites is shifted and the absolute values of the energy differences between the sites are reduced. Even if these calculations indicate an adsorption site which conflicts with experimental evidence for the lowest coverage structure, it should first be noted that the current energy differences among the sites are much smaller than those found in Ref. 41. Second, the energy differences are so small that zero-point vibrations and entropy corrections to the total energies might reverse the order of the sites. Third, core corrections of the order 50 meV to the total energy could possibly also alter the order. Inclusion of zero-point motion would involve calculation and diagonalization of the dynamical matrix of the entire slab, something which has not been done in the present work. Therefore the only conclusion that should be made from the above results is that there are no large energy differences (as compared to thermal or vibrational energies) involved when adsorbing in a hollow or bridge site instead of a on-top site.

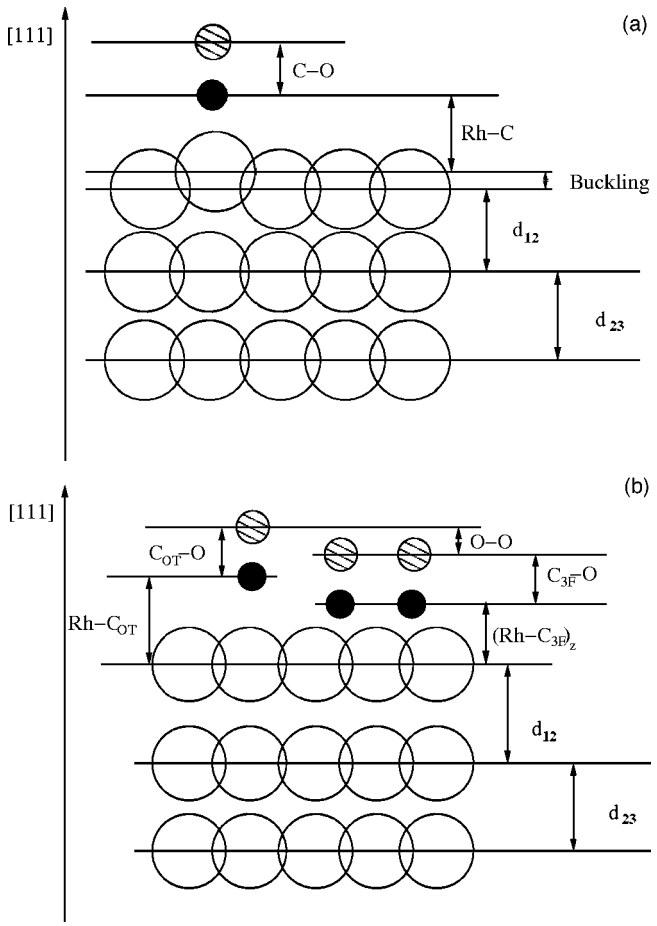

FIG. 3. All distances referred to in the tables of the calculated geometries in the low and high coverage limit.

TABLE II. Total (pseudo)energy differences compared to the on-top adsorption site for each over-layer. The adsorption sites can be seen in Fig. 2.

	Calculated value (eV)
The (2×2)-1CO system:	
on-top	0.0
hollow	-0.046
bridge	0.073
The $(\sqrt{3}\times\sqrt{3})R30°$-1CO system:	
on-top	0.0
hollow	0.017
bridge	0.070

TABLE III. Optimum geometrical parameters for the $(\sqrt{3}\times\sqrt{3})R30°$-1CO/Rh(111)-system (0.33 ML) An explanation to the distances are given in Fig. 3 and the adsorption sites are found in Fig. 2.

Distance	Adsorption site	Calculated value (Å)	Experimental value (Å) [a]	Code
Δd_{12}	on-top	-0.5%	-0.8%	fhi98md
Δd_{23}	on-top	0%	0.0%	fhi98md
C-O	on-top	1.15	1.20 ± 0.05	fhi98md
		1.16		Dacapo
C-Rh	on-top	1.86	1.87 ± 0.04	fhi98md
		1.84		Dacapo
Buckling	on-top	$+0.21$	0.08 ± 0.06	fhi98md
		$+0.23$		Dacapo
C-O	bridge	1.18		Dacapo
$(\text{C-Rh})_z$ [b]	bridge	1.49		Dacapo
C-O	hollow (hcp)	1.19		Dacapo
$(\text{C-Rh})_z$ [b]	hollow (hcp)	1.36		Dacapo

[a]Reference 6.

[b]The $(\text{C-Rh})_z$ distance is defined as the difference between the z coordinate of the C atom and an average of the z coordinates of the Rh atoms directly involved in the C-Rh bond.

TABLE IV. Optimum geometrical parameters for the (2×2)-1CO/Rh(111)-system (0.25 ML). No experimental data are available for this geometry. An explanation to the distances are given in Fig. 3 and the adsorption sites are found in Fig. 2.

Distance	Adsorption site	Calculated value (Å)	Code
Δd_{12}	on-top	-1.0%	fhi98md
Δd_{23}	on-top	-0.5%	fhi98md
C-O	on-top	1.16	fhi98md
		1.16	Dacapo
C-Rh	on-top	1.88	fhi98md
		1.83	Dacapo
Buckling	on-top	$+0.19$	fhi98md
		$+0.22$	Dacapo
C-O	bridge	1.18	Dacapo
$(\text{C-Rh})_z$ [a]	bridge	1.48	Dacapo
C-O	hollow (hcp)	1.19	Dacapo
$(\text{C-Rh})_z$ [a]	hollow (hcp)	1.36	Dacapo

[a]The $(\text{C-Rh})_z$ distance is defined as the difference between the z coordinate of the C atom and an average of the z coordinates of the Rh atoms directly involved in the C-Rh bond.

The small energy differences between differently adsorbed molecules indicate a very flat potential-energy surface (PES) for CO molecules on the Rh(111) surface, a fact which is verified experimentally.[10] In this HRCLS experiment it was found that the occupation of different sites depends on the temperature in a reversible way. This effect is particularly strong at molecular coverages around 0.5 ML. For coverages from ~0.4 to ~0.56 ML an increase of the temperatures results in a *decrease* of the CO molecules occupying on-top sites whereas for higher coverages an increase of the temperature from 100 to 300 K results in an *increased* on-top occupation. This indicates that the adsorption energy difference for different adsorption sites, even at low coverages, are in the range of the thermal energy kT, i.e. the PES is rather flat. The flatness of the PES and the implications of this will be further discussed in connection with the chemical shifts in Sec. III B. We now discuss each of the calculated geometries in more detail concentrating first on the geometry for the on-top adsorption structures.

We start by discussing the $(\sqrt{3}\times\sqrt{3})R30°$ overlayer since this is the one which has been determined experimentally.[6] This unit cell is depicted in Fig. 2. The full results for this geometry can be seen in Table III. According to our calculations the C atom sits 1.86 Å above the rhodium atom and the CO bond length is 1.15 Å in this overlayer. Further, we predict that the CO molecules induce a rather large outward buckling of the Rh atom directly under it. We calculate a value of 0.21 Å. This buckling could be compared with the calculations for a 0.25 ML of CO on a Rh(100) surface by Eichler *et al.*[16] They predict a value of 0.13 Å using similar computational tools as the present calculations. We can also compare our calculated values directly to available LEED data.[6] The calculated and experimental values for the Rh-C and the C-O bond lengths are seen to agree well while the calculated value for the buckling is somewhat too large when compared to experiment.

For the (2×2)-1CO system there are no data available for comparison but our calculations show that there are only minor changes in the relevant bond distances as compared to the $(\sqrt{3}\times\sqrt{3})R30°$ geometry. The (2×2)-1CO geometry is summarized in Table IV. Now the C atom sits 1.88 Å above the rhodium atom and the CO bond distance is 1.16 Å. The buckling does not change much and is here $+0.19$ Å. Even if there are no available geometrical data for this system, HRCLS measurements indirectly indicate that the buckling which is present in the $(\sqrt{3}\times\sqrt{3})R30°$ geometry also remains for the (2×2)-1CO system. The chemical shift of the Rh $3d$ level for the Rh atoms directly below the CO molecules is very similar for these two overlayers, which indicates similar bucklings, as will be further discussed in Sec. III B.

This resemblance between the 0.25- and 0.33-ML cases implies that the adsorbed molecules do not influence each other to any great extent in these low coverage structures. This fact has also been verified in a recent high-resolution electron energy-loss spectra (HREELS) experiment[46] where it was found that below approximately a coverage of 0.5 ML, the CO molecules interact only due to dynamic dipole-dipole couplings. For higher coverages, this study showed the existence of also a chemical part of the interaction, i.e., an overlap of the molecular wave functions. We therefore expect a larger influence of the surrounding molecules as we go to the high coverage limit.

For the case of adsorption in hollow and bridge sites, the C-O bond length is calculated to 1.19 Å in a (2×2) unit cell. Also in these adsorption situations rather large bucklings occur in the surface layer. In bridge adsorption there are two Rh

TABLE V. Optimum geometrical parameters for the (2×2)-3CO/Rh(111) system (0.75 ML). An explanation to the distances are given in Fig. 3.

Distance	Calculated value (Å)	Experimental value	Code
C_{3F}-O	1.18	1.17, [a]1.18 [b]	fhi98md
	1.18		Dacapo
C_{OT}-O	1.14	1.16, [a] 1.15 [b]	fhi98md
	1.15		Dacapo
$(C_{3F}\text{-Rh})_z$ [c]	1.48	1.49 ± 0.05, [a]1.47 ± 0.04 [b]	fhi98md
	1.45 [d]		Dacapo
	1.43 [e]		Dacapo
C_{OT}-Rh	1.87		fhi98md
	1.86		Dacapo
O-O	0.35	0.38 ± 0.07, [a]0.33 ± 0.07 [b]	fhi98md
	0.41 [d]		Dacapo
	0.43 [e]		Dacapo
Δd_{12}	+3.8%	+3% [a]	fhi98md
Δd_{23}	+0.0%	0.0% [a]	fhi98md

[a]Reference 8.
[b]Reference 6.
[c]The $(C\text{-Rh})_z$ distance is defined as the difference between the z coordinate of the C atom and an average of the z coordinates of the Rh atoms directly involved in the C-Rh bond.
[d]hcp three fold hollow.
[e]fcc three fold hollow.

atoms directly involved in the bonding to the CO molecule and in hollow adsorption there are three such atoms, as can be seen in Fig. 2. In Tables III and IV the $(C\text{-Rh})_z$ distance refers to the difference between the z coordinate for the C atom and an average of the z coordinates of these directly involved Rh atoms. In hollow adsorption we get a value of 1.36 Å for the $(C\text{-Rh})_z$ distance in the (2×2) unit cell while the corresponding value for bridge adsorption is 1.48 Å. These bond lengths are not changed much in a $(\sqrt{3}\times\sqrt{3})R30°$ geometry and the full results can be seen in Tables IV and III. Finally, we find small lateral movements (of the order of 0.01 Å) of Rh atoms away from the CO molecules, except for the $(\sqrt{3}\times\sqrt{3})R30°$ structure where such movements are not allowed by symmetry.

3. High coverage limit

In the high coverage limit we examined the (2×2)-3CO structure, which has one of its three CO molecules in an on-top position and the remaining two in the fcc and hcp three fold hollow positions. In the ultrasoft pseudopotential calculations we allowed these two hollow position molecules to relax independently. The results from this relaxation show that the bond differences are very small due to the fact that the local surroundings are very similar for the two hollow sites. Therefore we have chosen to treat them as identical when optimizing the geometry in the normconserving calculations.

There has been some controversy during the last ten years whether this (2×2)-3CO structure is the correct one but recent core-level photoemission measurements,[17] LEED analysis,[6] and surface x-ray experiments[8] all agree that this structure indeed is correct. There is no or very small buckling of the rhodium surface layer. Instead the surface relaxation of rhodium is affected. In the clean surface case the outermost layer relaxes inwards, however, for the (2×2)-3CO overlayer the top layer of the metal instead relaxes outwards.

Our calculations agree with the experimental finding of an outwards relaxation of the first Rh layer. We calculate a value of +3.8% which is slightly larger than measured. For the second layer the relaxation is negligible as also indicated by experiment.[8] We determine the on-top molecule to now sit 1.87 Å above its rhodium atom and the C-O bond length has decreased to 1.14 Å. For the threefold hollow adsorbed molecules the $(C\text{-Rh})_z$ distance is calculated to 1.48 Å and here the C-O bond length is 1.18 Å. For the threefold molecules the calculated $(C\text{-Rh})_z$ value correspond to a C-Rh bond length of 2.15 Å. These geometrical parameters agree very well with recent SXRD (Ref. 8) and LEED (Ref. 6) measurements. The full geometry is given in Table V.

TABLE VI. Rh 3*d* core-level shifts for the clean surface.

2D Supercell	Calculated value (eV)	Experimental value (eV)
(2×2)	−0.50	−0.50 [a]
$(\sqrt{3}\times\sqrt{3})R30°$	−0.52	−0.50 [a]
$(\sqrt{3}\times\sqrt{3})R30°$ without surface relaxation	−0.46	
2nd layer $(\sqrt{3}\times\sqrt{3})R30°$	+0.01	
3rd layer $(\sqrt{3}\times\sqrt{3})R30°$	0.00	

[a]Reference 10.

TABLE VII. CO induced Rh $3d$ shifts.

2D supercell	Atom	Calculated value (eV)	Experimental value (eV) [a]	Code
(2×2)-1CO:				
	Rh_{OT}	0.29	0.27	fhi98md
	Rh_{OT} *without* buckling	0.49		fhi98md
$(\sqrt{3}\times\sqrt{3})R30°$-1CO:				
	Rh_{OT}	0.24	0.27	fhi98md
	Rh_{Cln}	−0.52	−0.50	fhi98md
(2×2)-3CO:				
	Rh_{OT}	0.26	0.24	fhi98md
	Rh_{OT} *without* surface relaxation	0.30		fhi98md
	Rh_{3F}	−0.22	−0.16	fhi98md

[a]Reference 10.

B. Chemical shifts

Following the experimental practice we give all shifts as changes in binding energies $(-\epsilon_c)$. The shifts in Rh $3d$ binding energy we refer to the bulk, i.e.,

$$\Delta_c = -(\epsilon_c^{(\mathrm{Surface})} - \epsilon_c^{(\mathrm{Bulk})}). \tag{10}$$

The bulk value of the $3d$ level is obtained by ionizing a rhodium atom in the middle of the slab. Depending on whether we use a symmetric or a dipole corrected slab we obtain values for the bulk binding energy which differ slightly, of the order of 50 meV. To improve consistency we therefore use the same type of slab (symmetric or dipole corrected) for both the shifted and the reference bulk core level.

In the case of shifts of the $1s$ level of the carbon atom in CO molecules due to different geometrical configurations, the context will show to what reference system the shifts refer. Our calculated shifts are given in Tables VI–X. We have not performed estimates of possible core corrections to all the results given below. Our test discussed in Sec. II C indicates corrections of the order 0.04 eV for the Rh 3d level and even smaller corrections for C $1s$.

1. Clean surface

For the clean surface the SCLS was calculated using a (2×2) surface unit cell for the ionized Rh atoms. We obtained a value of -0.50 eV which agrees very well with experiment.[10] The corresponding value when using a $(\sqrt{3}\times\sqrt{3})R30°$ surface unit cell is -0.52 eV. The close resemblance between the (2×2) and $(\sqrt{3}\times\sqrt{3})R30°$ values shows that the two-dimensional (2D) supercell is large enough for interactions between core holes in different cells to play only a minor role. This short screening length of Rh metal also manifests itself in the core-level binding-energy shift of the second atomic layer of the Rh(111) surface. Using a $(\sqrt{3}\times\sqrt{3})R30°$ supercell we calculate a value for this shift of 0.01 eV, i.e., to within 10 meV the Rh $3d$ level of the second layer is identical to the level of bulk Rh. As can be seen in Fig. 4 the SCLS of clean Rh(111) arises almost entirely from the initial-state shift in core eigenvalue.

A number of previous calculations are available of the SCLS of clean Rh(111). Feibelman using an LCAO approach[11] calculated a value of -0.6 eV in the initial-state approximation. Later Andersen *et al.*[14] employing an LDA based full potential LMTO method and using a (2×2) unit cell for the ionized atoms calculated values of -0.42 eV and -0.54 eV for surfaces with first interlayer contractions of -2.5% and 0%, respectively. Recently, Ganduglia-Pirovano *et al.*[47] using the LAPW method, GGA and a 2×2 supercell obtained -0.46 eV in excellent agreement with our corresponding all-electron result, and also with our plane-wave results when a core correction of $+0.03$ eV is applied. The small differences between the present results and those of Ref. 14 are most probably caused by slight differences in the geometry, that is, of the interlayer distances in the surface. When calculating the SCLS using a $(\sqrt{3}\times\sqrt{3})R30°$ supercell without any relaxation we obtain a value of -0.46 eV which may be compared to a value of -0.52 eV for the fully relaxed geometry. Thus small changes of the order of 1% in the interlayer distances induce changes of the calculated SCLS of the order of 60 meV, i.e., of a magnitude comparable to the differences among the values calculated in different studies. In this connection it may also be noted that experimentally observed changes of the SCLS of the

TABLE VIII. Calculated C $1s$ shifts in the low coverage systems. All shifts are relative to the level of the C atom in an on-top position in the (2×2)-1CO system. All calculations have been made with the Dacapo code.

	Core ionized PP (eV)	$Z+1$ approx. (eV)
(2×2)-1CO:		
on-top	0.00	0.00
hollow	−0.68	−0.44
bridge	−0.53	−0.37
$(\sqrt{3}\times\sqrt{3})R30°$-1CO:		
on-top	−0.01	−0.01
hollow	−0.69	−0.46
bridge	−0.52	−0.37

TABLE IX. C 1*s* shifts in the high coverage limit.

	Calculated value (eV)	Z+1	Experimental value (eV)	Code
On-top–three fold hollow	−0.73	−0.53	−0.65, [a] -0.70 [b]	fhi98md
On-top–three fold hollow	−0.56	−0.32		dacapo
On-top (2×2)-1CO–on-top	−0.02		−0.07 [a], −0.05 [b]	fhi98md
On-top (2×2)-1CO–on-top	−0.09	−0.14		dacapo

[a]Reference 10.
[b]Reference 18.

Rh(100) with temperature were interpreted as caused by an expansion of the first interlayer distance with increasing temperature.[48]

The reason why the core-level binding-energy shifts may be quite sensitive to the interlayer distance in particular or to any geometrical parameter in general is illustrated in Fig. 5. This figure shows schematically the potential energy variation with a geometrical parameter (e.g., the interlayer distance) of the initial and the final state atom. In general, these two potential-energy curves will not have their minima at the same value of the geometrical parameter. As photoemission is a vertical process in configuration space, ionization of an atom in the initial-state equilibrium position will in general lead to a final state which is far from geometrical equilibrium. Thus the final-state atom will end up on a quite steep part of the potential-energy curve whereby any small change of the geometry will cause a large change of the final-state total energy. As the same change of geometry only induces a small change of the initial-state total energy the resulting effect will be a large core-level binding-energy shift. A similar line of reasoning suggests to use the additional information given by the experimental value of the core-level shifts as a means to reduce the uncertainty of the geometrical structure determination. As illustrated in Fig. 5, small numerical instabilities (E1 in Fig. 5) may result in comparatively large uncertainties of the geometrical parameters for the initial state as the potential-energy curves are rather flat close to the minimum. In the final state, this uncertainty in geometrical parameters will, however, often result in energy differences (E2 in Fig. 5) considerably larger than the numerical accuracy.

2. Low coverage limit

We now turn to the systems at low coverages, namely the (2×2)-1CO and $(\sqrt{3}\times\sqrt{3})R30°$-systems (cf. Fig. 2). At these coverages only on-top adsorption has been clearly identified experimentally, and we begin our discussion with this case. With CO adsorbed on top there will be two inequivalent Rh atoms in the surface layer. We denote the Rh atom directly under the CO molecule by Rh_{OT} and the other Rh atoms in the surface unit cell by Rh_{Cln} (see Fig. 2).

When optimizing the geometry for on-top adsorption at low coverage we found a rather large buckling of the surface layer of the metal. As in the clean-surface case we find that the core energies depend on the local geometry quite strongly, and the buckling is crucial for obtaining the correct CO induced SCLS for Rh_{OT}. We see in Table VII that the CO-induced shifts with buckling agree rather well with experiment for both (2×2)-1CO and $\sqrt{3}\times\sqrt{3})R30°$. Without buckling we find a CO induced shift of 0.49 eV for the Rh_{OT} $3d$ level in the (2×2)-1CO system. When the surface is allowed to deform, the shift reduces by 0.20–0.29 eV in close agreement with the experimental value 0.27 eV.[10] Although this change in the shift is much larger than in the clean surface case, we should keep in mind that the distances involved in the buckling are substantially larger than the distances involved in the relaxation of the clean surface.

In the case of the clean surface, we found that the Rh core shift was dominated by changes in the initial-state Hartree potential. In Fig. 4 we see that the CO-induced shift of the Rh_{OT} atom has exactly the opposite behavior and originates almost entirely from changes in relaxation.

The Rh_{Cln} atoms have local surroundings very similar to those of surface atoms on a clean surface and one would therefore expect these atoms to have a core-level binding energy similar to the clean surface value. This expectation is confirmed for the $(\sqrt{3}\times\sqrt{3})R30°$ system where we calculate a $3d$ shift of the Rh_{Cln} atoms which is equal to the SCLS of the clean surface to within the computational accuracy.

In summary we find a quite satisfying agreement between theoretical and measured Rh core shifts for the (2×2)-1CO and $\sqrt{3}\times\sqrt{3})R30°$ systems, but only if the correct geometrical parameters are used. On the basis of this good agreement we believe that the rather large buckling obtained here is a genuine effect. In the $(\sqrt{3}\times\sqrt{3})R30°$ system we obtain a Rh_{OT} shift of 0.24 eV which is slightly

TABLE X. O 1*s* shifts.

	Calculated value (eV)	Experimental value (eV)	Code
On-top–threefold hollow in (2×2)-3CO	1.44	1.60	fhi98md

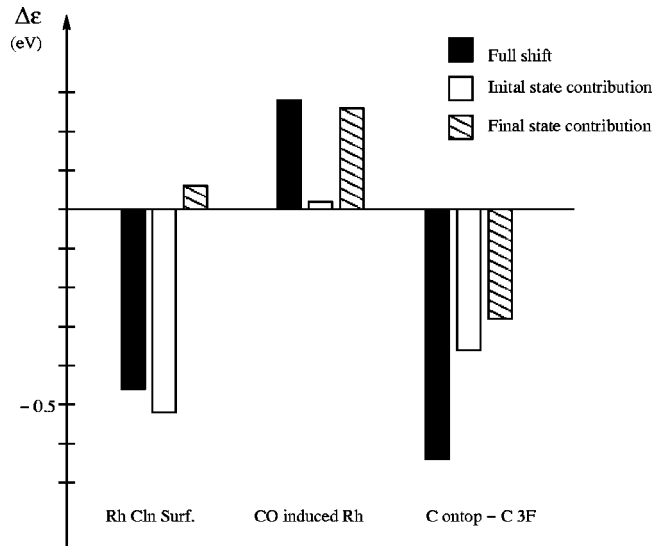

FIG. 4. Initial- and final-state decomposition of the chemical shifts for the Rh 3*d* level for the clean Rh surface (left) and the (2×2)-1CO system (middle), and for the C 1*s* level for the (2×2)-3CO system (right).

smaller than the corresponding shift in the (2×2)-1CO system (0.29 eV), whereas experiment[10] gives the same value (0.27 eV) for both. This deviation could possibly be an artifact of too small surface a unit cell for the ionized $(\sqrt{3}\times\sqrt{3})R30°$ system, although our other results suggest a very short screening length for core holes in Rh. Finally, the computational result that the Rh_{Cln} atoms have a 3*d* binding energy very close to that of the clean surface Rh atoms also agrees with experiment[10] which could not resolve any 3*d* shift away from the clean surface position of the Rh_{Cln} atoms in the (2×2)-1CO and the $(\sqrt{3}\times\sqrt{3})R30°$ structures. The results for the low coverage structures demonstrate clearly that the CO induced core-level binding-energy shifts of the Rh 3*d* level to a very good approximation are determined by the local geometry. The good agreement is obtained with the computed rather than the experimental buckling. In the case of the $\sqrt{3}\times\sqrt{3})R30°$ system this casts some doubt on the value derived from LEED measurements.

We next turn to the C 1*s* binding-energy shifts at low coverage. In addition to the experimentally observed on-top adsorption site, we have also performed calculations for hypothetical bridge and threefold-hollow adsorption sites in the (2×2)-1CO and $(\sqrt{3}\times\sqrt{3})R30°$ systems. Our results are given in Table IX. For the on-top adsorption we find a small C 1*s* shift towards lower binding energy when going from the (2×2)-1CO to the $(\sqrt{3}\times\sqrt{3})R30°$ system. A similar shift is observed experimentally,[18] however, we would consider this agreement somewhat fortuitous as the shift is definitely below the computational accuracy in particular as different supercells are used in the two calculations. The shifts resulting from changing the adsorption site are on the other hand quite large. Moving the CO molecules to a threefold-hollow site results in a lowering of the C 1*s* binding energy from the on-top value by about 0.7 eV for both the (2×2)-1CO and the $(\sqrt{3}\times\sqrt{3})R30°$ overlayer. An on-top to threefold-hollow C 1*s* shift of this magnitude is expected from measurements[10,18] on the (2×2)-3CO structure where both adsorption sites are occupied. As will be discussed later, calculations for the (2×2)-3CO structure also lead to a similar C 1*s* shift. Shifting the adsorption site from on-top to bridge also induces a quite large lowering of the C 1*s* binding energy of about 0.5 eV. In a recent experimental study, Smedh *et al.*[18] identified a C 1*s* component with a binding energy about 0.5 eV below the on-top component and tentatively assigned this component to emission from CO molecules in bridge sites. Even though the present calculations are not performed at the coverages where the bridge compo-

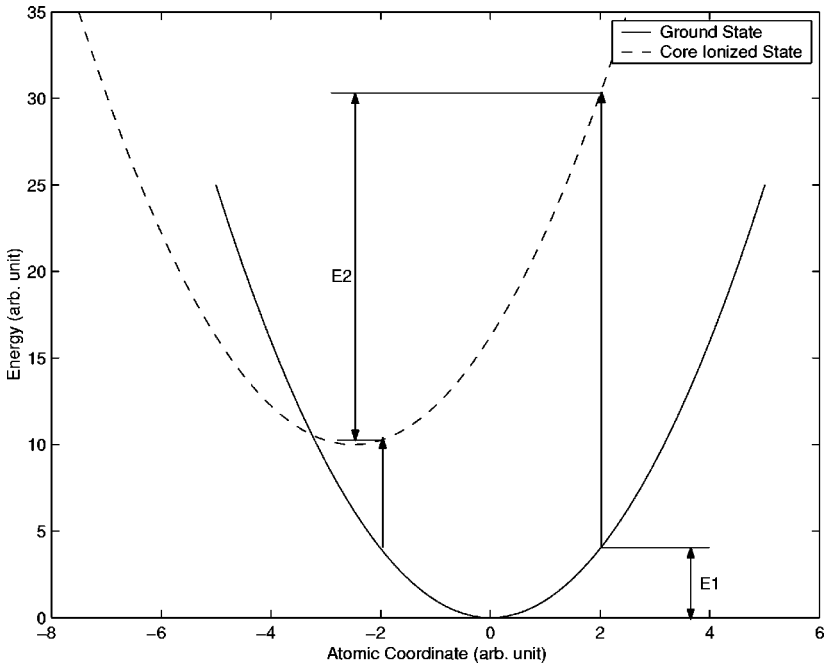

FIG. 5. An energy uncertainty E1 for the ground state may correspond to a much larger energy difference E2 for the core-excited state.

nent is found experimentally we still believe that the calculated C 1*s* shifts for a hypothetical bridge site in the (2 $\times$2)-1CO and ($\sqrt{3}\times\sqrt{3}$)*R*30° structures provide strong support for the interpretation of Smedh *et al.* as we in general find the C 1*s* binding energy shifts to be dominated by the coordination to Rh atoms whereas the existence of nearby CO molecules has only a minor influence.

These results for the C 1*s* binding-energy shifts nicely illustrate the previously discussed usefulness of inclusion of the core-level binding-energy shifts as additional information in a DFT based determination of the geometry. As mentioned earlier, the CO adsorption site cannot be unambiguously determined for the present adsorption system due to the small energy differences between adsorption in the high-symmetry sites (see Sec III B 1). In contrast to the adsorption energies, the C 1*s* core-level binding energy, however, depends strongly on the adsorption site and comparison to the experimental C 1*s* binding-energy shifts unambiguously leads to identification of an on-top site in the low coverage (2 $\times$2)-1CO and ($\sqrt{3}\times\sqrt{3}$)*R*30° structures. The quite flat PES for the initial-state CO molecule mentioned earlier in combination with the large calculated C 1*s* shifts, indicates a strongly corrugated PES for the final state C 1*s* ionized molecule. In a $Z+1$ approximation perspective this implies a favoring of threefold-hollow adsorption for the NO/Rh(111) system. However, as can be seen in Table VIII, the $Z+1$ gives only qualitative results in the present case. The C 1*s* core level is also not a very good candidate for this kind of approximation. Owing to the absence of core states of *p* symmetry, the *p*-wave part of the valence-electron orbitals penetrates into the core region. Inside the core region, an ionized C atom and a N atom are of course quite different. It is thus not surprising that the equivalent core approximation is inaccurate in this case. The absence of *p* states in the core also makes the pseudopotential approximation somewhat questionable. In order to verify the validity of our approximations we have also calculated shifts and corresponding $Z+1$ results using the LAPW method. The agreement between the all-electron and pseudopotential results are within 50 meV.

3. High coverage limit

Neglecting the difference between fcc and hcp sites, there are two types of CO molecules in the (2$\times$2)-3CO structure, on-top and threefold-hollow, which we designate CO_{OT} and CO_{3F}, as indicated in Fig. 2. As in the low coverage case, the unit cell in the high coverage limit contains two inequivalent types of Rh atoms in the surface layer when the difference between the threefold-hollow adsorbed CO molecules is neglected. One type of Rh sits directly below an on-top CO molecule and the other type bonds to two CO molecules in threefold-hollow sites. As illustrated in Fig. 2, we use the designation Rh_{OT} and Rh_{3F} for these two types of Rh atoms. From the difference in the local geometry we expect different CO induced shifts of the Rh_{OT} and Rh_{3F} atoms as well as different C (and O) 1*s* binding energies of the CO_{OT} and CO_{3F} molecules. This is also what has been found experimentally.[10]

In the systems discussed previously we found a rather strong dependence of the core-level shifts on the local geometry. We have not made a complete investigation of these effects at high coverages. However, in order to get an impression of the magnitude of the geometry dependence we calculated the 3*d* shift of the Rh_{OT} atom for values of the first interlayer spacing d_{12} corresponding to both the optimum expansions of +3.8% as well as using the bulk interlayer distance for d_{12} (0.0% expansion). For no expansion we get a Rh_{OT} shift of +0.30 eV whereas use of the optimum geometry yields a Rh_{OT} shift of +0.26 eV, that is, a weaker dependence on the first layer relaxation than found for the clean surface in a previous section. The binding-energy shifts given below are all obtained for the optimum geometry obtained by fhi98md as given in Table V.

The calculated CO induced 3*d* shifts are presented in Table VII. Experimentally these shifts are difficult to determine with high precision as the shifts are of similar magnitude as the Rh 3*d* line width thus making the Rh 3*d* spectrum rather broad and featureless. However, experimental values of about +0.24 and −0.16 eV have been reported[10] for the Rh_{OT} and Rh_{3F} atoms, respectively, which also agree with more recent measurements[49] at higher energy resolution. These experimental values are seen to be in good agreement with the calculated values.

The Rh_{OT} shift for the (2$\times$2)-3CO structure is very similar to that found for the low coverage structures. This may seem surprising as the buckling of the first Rh layer, which had a major influence on the Rh_{OT} shift for these low coverage structures, disappears almost entirely in the (2 $\times$2)-3CO structure. However, the increase of the shift expected from this disappearance of the buckling is counteracted by a decrease of the shift induced by the outward relaxation of the entire first Rh layer and by the addition of the CO_{3F} molecules in the (2$\times$2)-3CO structure. By calculating the Rh_{OT} shift for a number of hypothetical intermediate geometries we found that the reductions caused by these two effects are of approximately equal magnitude ($\sim$0.15 eV).

The ordering of the CO induced Rh_{OT} and Rh_{3F} shifts is expected from arguments based on the $Z+1$ approximation. The adsorbate induced shift relative to the clean surface value is related to the difference in adsorption energy on the Z and the $Z+1$ metal, see, e.g., Ref. 50 and references therein. As there are only small CO adsorption energy differences among the on-top and the threefold-hollow sites on Rh(111) and as the preferred adsorption site of CO on the $Z+1$ equivalent of Rh, Pd, is threefold-hollow and not on-top,[51–53] indicating a lower CO adsorption energy in the on-top site on Pd, the CO induced shift of the Rh_{OT} should be the larger one.

Concerning the C 1*s* level we calculate that the binding energy of the CO_{OT} molecule is 0.7 eV higher than that of the CO_{3F} molecule. The shift is decomposed into initial- and final-state contributions in Fig. 4, and we see that the two contributions are of about equal importance. The calculated shift is in good agreement with an experimental value of 0.65 eV.[10] In a more recent experimental study[18] at higher resolution, a value of 0.70 eV was reported. This value, however, refers to the difference between the vibrationally adiabatic

peaks and is therefore not directly comparable to the presently calculated value which refers to a vertical transition. Correcting the experimental value by use of the experimental vibrational splittings and intensity distributions one arrives at an experimental value of 0.65 eV for the vertical energy in perfect agreement with the previously obtained experimental value.[10] Finally we also calculated the O 1*s* binding-energy shifts of the CO_{OT} and CO_{3F} molecules and obtained a value of 1.45 eV again with the on-top molecule having the larger 1s binding energy. Also this value is in good agreement with an experimental value of $\sim$1.6 eV.[49]

Assuming a rather uncorrugated PES for the initial state CO molecules this ordering of the C 1*s* binding energies and the large shift, as discussed earlier, demonstrates a strong tendency of adsorbed NO to occupy threefold-hollow as opposed to on-top sites in agreement with experimental findings.[54]

Finally, we may compare the C 1*s* binding energies of the on-top molecules in the low coverage (2×2)-1CO and the present high coverage (2×2)-3CO structures. Even though there is some difference in the results obtained by the two computational methods (see Table IX) we still find that the calculations reproduce the experimental findings of a small C 1*s* binding energy decrease by 70 (Ref. 10) or 50 meV (Ref. 18) from the (2×2)-1CO to the (2×2)-3CO overlayer.

From the small magnitude of the CO_{OT} shift between the (2×2)-1CO and the (2×2)-3CO structures and similar small shifts observed in CO-O or K co-adsorption systems[55,56] it has been argued that the C 1s binding energy provides a good fingerprint of the adsorption site in pure and co-adsorbed CO overlayers as it is rather insensitive to the presence of nearby adsorbed molecules/atoms. Of course, the CO_{OT} shift between the two (2×2) structures contains two parts, one related to the change in number of neighboring CO molecules and one related to the changes in the Rh geometry, i.e., the rumpling and the first interlayer distance and the observed small total shift could *a priori* be a result of two large but canceling partial shifts. In order to isolate the contribution caused by the addition of two CO molecules per unit cell we performed calculations for a geometrically constrained (2×2)-1CO overlayer formed by simply removing the threefold-hollow CO molecules from a (2×2)-3CO overlayer. These yielded a CO_{OT} binding energy 70 meV higher than that of the (2×2)-3CO structure demonstrating that, although some cancellation occurs between the CO and the Rh related parts of the total shift, the influence of adding two additional CO molecules per (2×2) unit cell on the CO_{OT} C 1*s* binding energy is quite small.

IV. CONCLUSIONS

The present paper describes the use of density-functional theory based calculations for determining geometries and core-level binding energies in CO on Rh(111) adsorption systems. A brief discussion is also given of some issues related to the interpretation of DFT and HF energy eigenvalues and of problems related to the nontransferability of total energies in pseudopotential schemes.

Concerning the geometry obtained by minimization of the total energy the results compare favorably with experimental values in the cases where such exist, i.e., for the clean surface, for the $(\sqrt{3}\times\sqrt{3})R30°$-1CO, and the (2×2)-3CO overlayers. Deviations from the experimental values are in all cases smaller than the quoted experimental uncertainties except for the CO induced buckling of the outermost Rh layer in the $(\sqrt{3}\times\sqrt{3})R30°$-1CO system. For this system, the DFT calculations predict a larger corrugation than found experimentally. However, the deviation from the experimental value is below 0.15 Å to be compared to an estimated experimental uncertainty of 0.06 Å. A substantial CO induced buckling is also predicted for the (2×2)-1CO system where no experimental determination has been performed of the geometrical structure. Finally, the DFT calculations turn out to be inconclusive when it comes to determining the adsorption sites of the CO molecules. For the $(\sqrt{3}\times\sqrt{3})R30°$ and the (2×2)-1CO structures we find indications of a very flat potential energy surface with only small adsorption energy differences for CO molecules in the high-symmetry sites.

The core-level binding-energy shifts are found to be well described by the calculations. This applies to the shifts of the substrate levels as well as to the shifts of the C 1*s* level of the CO adsorbates. The obtained level of agreement between experimental and calculated core-level binding-energy shifts, however, demands that the correct geometrical parameters are used, e.g., inclusion of the first layer bucklings in the (2×2)-1CO and $(\sqrt{3}\times\sqrt{3})R30°$-1CO overlayers was essential. Specifically, the calculated CO induced shifts of the Rh 3*d* binding energy for the (2×2)-1CO and $(\sqrt{3}\times\sqrt{3})R30°$ structures were found to be incompatible with the experimental value if no rumpling of the Rh layer was included. This fact provides additional support to the aforementioned prediction of a substantial buckling also for the (2×2)-1CO overlayer. In case of the C 1*s* binding energy we find large differences between CO adsorbed in different sites. Thus calculations of the C 1*s* binding energy allow us to predict the adsorption sites even for the overlayers where the CO adsorption energies are almost degenerate for the different adsorption sites. The present calculations also provide support to a recent claim[18] that bridge bonded CO exists on Rh(111) at intermediate coverages. Finally, the calculations allow us to examine more closely the details of the core-level shifts by making calculations for hypothetical geometrically constrained systems. This for instance confirmed the experimental finding that the C 1*s* binding energy is mainly determined by the adsorption site whereas the existence of nearby adsorbed CO molecules has only minor influence. Finally a number of explicit examples were given of decompositions of the calculated core level binding-energy shifts into initial- and final-state contributions. These examples clearly show that a large variation exists in the relative importance of initial- and final-state effects, exemplifying the dangers of interpreting core-level binding-energy shifts in a simple initial-state framework.

ACKNOWLEDGMENTS

This work has been financially supported by the Swedish Natural Science Research Council.

*Electronic address: Martin.Birgersson@teorfys.lu.se
†Electronic address: Carl-Olof.Almbladh@teorfys.lu.se
†Electronic address: Mikael.Borg@sljus.lu.se
§Electronic address: Jesper.Andersen@sljus.lu.se

[1] P. Hohenberg and W. Kohn, Phys. Rev. **136**, B864 (1964).
[2] W. Kohn and L. J. Sham, Phys. Rev. **140**, A1133 (1965).
[3] C.-O. Almbladh and L. Hedin, in *Handbook on Synchrotron Radiation*, edited by E. E. Koch (North-Holland, Amsterdam, 1983), Vol. 1b, p. 607.
[4] J. N. Andersen and C.-O. Almbladh, J. Phys.: Condens. Matter **13**, 11 267 (2001).
[5] D. G. Castner, B. A. Sexton, and G. A. Somorjai, Surf. Sci. **71**, 519 (1978).
[6] M. Gierer, A. Barbieri, M. A. van Hove, and G. A. Somoraji, Surf. Sci. **391**, 176 (1997).
[7] L. H. Dubois and G. A. Somorjai, Surf. Sci. **91**, 514 (1980).
[8] E. Lundgren, X. Torrelles, J. Alvarez, S. Ferrer, H. Over, A. Beutler, and J. N. Andersen, Phys. Rev. B **59**, 5876 (1999).
[9] H. Over, S. Schwegmann, G. Ertl, D. Cvetko, V. D. Renzi, L. Floreano, R. Gotter, A. Morgante, M. Pelio, F. Tommasini, and S. Zennaro, Surf. Sci. **376**, 177 (1997).
[10] A. Beutler, E. Lundgren, R. Nyholm, J. N. Andersen, B. Setlik, and D. Heskett, Surf. Sci. **396**, 117 (1998).
[11] P. J. Feibelman, Phys. Rev. B **26**, 5347 (1982).
[12] M. Methfessel, D. Hennig, and M. Scheffler, Phys. Rev. B **46**, 4816 (1992).
[13] O. K. Andersen, Phys. Rev. B **12**, 3060 (1975).
[14] J. N. Andersen, D. Hennig, E. Lundgren, M. Methfessel, R. Nyholm, and M. Scheffler, Phys. Rev. B **50**, 17 525 (1994).
[15] A. Eichler, J. Hafner, J. Furthmuller, and G. Kresse, Surf. Sci. **346**, 300 (1996).
[16] A. Eichler and J. Hafner, J. Chem. Phys. **109**, 5585 (1998).
[17] A. Beutler, E. Lundgren, R. Nyholm, J. Andersen, B. Setlik, and D. Heskett, Surf. Sci. **371**, 381 (1997).
[18] M. Smedh, A. Beutler, T. Ramsvik, R. Nyholm, M. Borg, J. N. Andersen, R. Duschek, M. Sock, F. P. Netzer, and M. G. Ramsey, Surf. Sci. **491**, 99 (2001).
[19] C.-O. Almbladh and U. von Barth, Phys. Rev. B **13**, 3307 (1976).
[20] N. D. Lang and A. R. Williams, Phys. Rev. B **16**, 2408 (1977).
[21] P. J. Feibelman, Phys. Rev. B **39**, 4866 (1989).
[22] B. Johansson and N. Mårtensson, Phys. Rev. B **21**, 4427 (1980).
[23] N. Mårtensson and A. Nilsson, in *Application of Synchtrotron Radiation*, edited by W. Eberthardt (Springer, Berlin, 1994).
[24] C.-O. Almbladh and U. von Barth, in *Density Functional Methods in Physics*, edited by R. M. Dreizler and J. da Providência (Plenum, New York, 1985).
[25] L. Hedin and A. Johansson, J. Phys. B **2**, 1336 (1969).
[26] R. Manne and T. Åberg, Chem. Phys. Lett. **7**, 282 (1970).
[27] L. Hedin, Ark. Fys. **30**, 231 (1965).
[28] J. F. Janak, Phys. Rev. B **18**, 7165 (1978).
[29] M. Bockstedte, A. Kely, J. Neugebauer, and M. Scheffler, Comput. Phys. Commun. **107**, 187 (1997).
[30] B. Hammer, K. W. Jacobsen, V. Milman, and M. C. Payne, J. Phys.: Condens. Matter **4**, 453 (1992).
[31] U. von Barth and R. Car (unpublished).
[32] U. von Barth and A. C. Pedroza, Phys. Scr. **32**, 353 (1985).
[33] D. R. Hamann, M. Schlüter, and C. Chiang, Phys. Rev. Lett. **43**, 1494 (1979).
[34] N. Troullier and J. L. Martins, Phys. Rev. B **43**, 1993 (1991).
[35] D. Vanderbilt, Phys. Rev. B **41**, 7892 (1990).
[36] J. P. Perdew, J. Chevary, S. Vosko, K. A. Jackson, M. R. Pederson, D. Singh, and C. Foilhais, Phys. Rev. B **46**, 6671 (1992).
[37] J. Neugebauer and M. Scheffler, Phys. Rev. B **46**, 16 067 (1992).
[38] H. J. Monkhorst and J. D. Pack, Phys. Rev. B **13**, 5188 (1976).
[39] M. Gillan, J. Phys.: Condens. Matter **1**, 689 (1989).
[40] P. E. Blöchel, O. Jepsen, and O. K. Andersen, Phys. Rev. B **49**, 16 223 (1994).
[41] A. Barbieri, M. van Hove, and G. A. Somorjai, in *The Structure of Surfaces IV*, edited by X. D. Xie, S. Y. Tong, and M. A. van Hove (World Scientific, Singapore, 1994), p. 201.
[42] A. Wander, C. Barnes, L. Malpedoram, and D. King, Surf. Sci. **42**, 1993 ().
[43] S. Hengrasmee, K. Mitchell, P. Watson, and S. White, Can. J. Phys. **58**, 200 (1980).
[44] N. W. Ashcroft and N. D. Mermin, *Solid State Physics* (Saunders Collage Publishing, New York, 1976).
[45] P. J. Feibelman, B. Hammer, J. K. Norskov, F. Wagner, M. Scheffler, R. Stumpf, R. Watwe, and J. Dumesic, J. Phys. Chem. B **105**, 4018 (2001).
[46] R. Linke, D. Curulla, M. J. P. Hopstaken, and J. Niemantsverdriet, J. Chem. Phys. **115**, 8209 (2001).
[47] M. Ganduglia-Pirovano, M. Scheffler, A. Baraldi, S. Lizzit, G. Comelli, G. Paulucci, and R. Rosei, Phys. Rev. B **63**, 205415 (2001).
[48] A. Baraldi, C. Comelli, S. Lizzit, R. Rosei, and G. Paolucci, Phys. Rev. B **61**, 12 713 (2000).
[49] M. Smedh, A. Beutler, R. Nyholm, M. Borg, and J. N. Andersen (unpublished).
[50] J. W. F. Egelhoff, Surf. Sci. Rep. **6**, 253 (1986).
[51] A. M. Bradshaw and F. Hoffmann, Surf. Sci. **72**, 513 (1978).
[52] F. Hoffmann, Surf. Sci. Rep. **3**, 107 (1983).
[53] W. K. Kuhn, J. Szanyi, and D. Goodman, Surf. Sci. Lett. **274**, L611 (1992).
[54] I. Zasada, M. van Hove, and G. Somorjai, Surf. Sci. **418**, L98 (1998); note that these results lead to a reinterpretation of Ref. 57.
[55] A. J. Jaworowski, A. Beutler, F. Strisland, R. Nyholm, B. Setlik, D. Heskett, and J. N. Andersen, Surf. Sci. **431**, 33 (1999).
[56] F. Strisland, A. Beutler, A. J. Jaworowski, R. Nyholm, B. Setlik, D. Heskett, and J. N. Andersen, Surf. Sci. **410**, 330 (1998).
[57] C. Kao, G. Blackman, G. S. M. A. van Hove, and C. Chan, Surf. Sci. **224**, 77 (1989).
[58] As an example of this, in the Ne atom the 1s excitation energy is −870.2 eV, the HF eigenvalue −891.7 eV, the DFT eigenvalue −835.2 eV, and its LDA counterpart −824.7 eV.